DECOMPOSITION OF RADAR POLARISATION SIGNATURES FROM BUILT AND NATURAL TARGETS*

Y. Dong (Research Associate), B. C. Forster (Professor) and C. Ticehurst (PhD Candidate)
School of Geomatic Engineering, The University of New South Wales
Sydney NSW 2052, Australia
Telephone: + 61 2 385 4177, Facsimile: + 61 2 313 7493
Email: yunhan@fatboy.geog.unsw.edu.au

Commission VII, Working Group 1

KEY WORD: SAR, Modelling, Intepretation.

ABSTRACT

A method of optimal decomposition of radar polarisation signatures is developed. In the model the backscattering consists of single (odd), double, Bragg and cross backscattering components, and the Mueller matrix is the sum of the Mueller matrices of these four scattering mechanisms. The technique of Weighted Least Squares is then used to find the optimal combination of these four components. Using NASA/JPL AirSAR data, the results of the decomposition are compared with built and natural targets and found to agree with the general understanding of radar backscatter. The distinct decomposition of polarisation signatures can be used as a basis for land use classification.

1 INTRODUCTION

Quad-polarised SAR (Synthetic Aperture Radar) data such as that acquired and produced by NASA/JPL AirSAR system, give more information about the ground targets than single polarised SAR data. Excellent work has been done on modelling and classification of polarimetric radar backscatter for both built and natural targets (Freeman and Durden, 1992, van Zyl, 1989, Pierce et al., 1994, Cloude, 1991, Kwok et al., 1994, Zebker and van Zyl, 1991, Durden et al., 1991, Evans et al., 1988, and Ulaby and Elachi, 1990). Freeman and Durden (1992) present a three-component model in which three scattering mechanisms, i.e., volume scattering, double bounce scattering and surface scattering are included. The contribution of each mechanism is then estimated by solving four equations with five unknowns using the elements of the measured Mueller matrix. One of the unknowns is assigned a constant in order to solve the equations. A technique is given by van Zyl (1989) for unsupervised classification of scattering behaviour by selecting the dominant scattering mechanism. Each pixel is classified as either an odd number of reflections (small phase difference between HH and VV), even number of reflections (larger phase difference between HH and VV), or diffuse scattering (little correlation between HH and VV) by analyzing the elements of the measured Mueller matrix. Using image information such as co- and cross-polarised backscattering coefficients and the phase difference between HH and VV responses available in polarimetric data, Pierce et al. (1994) build a knowledge-based classifier. Pixels are then classified into four categories: tall vegetation, short vegetation, urban and bare soil.

The observed radar polarisation signatures are not very similar to the constructed polarisation signatures developed using only the one of simple scattering mechanisms. It reveals that the observed radar response is a combination of responses from various mechanisms. Since different scattering mechanisms give different polarisation signatures, they could be extracted from the measured Mueller matrix. This paper proposes an approach to decompose the polarisation signature observed by radar into a combination of scattering contributions by four basic scattering mechanisms. These four basic mechanisms are (1) double bounce scattering, (2) Bragg scattering, (3) single (odd) bounce scattering and (4) cross scattering, which form six equations with four unknowns plus four boundary conditions. The WLS (Weighted Least Squares) technique is used to find the optimal solutions. The approach is applied to different categories of images including forest, farmland, ocean and urban areas, and the results are discussed. The reconstructed polarisation signatures are seen to coincide very well with the observed signatures. It seems that a better understanding of these scattering mechanisms will assist in classification of land cover types from radar image data.

*This work was supported by the Australian Research Council.

2 BASIC SCATTERING MECHANISMS

Since positions of scatterers are randomly distributed, radar measurements for N independent scattering mechanisms can be added incoherently (Van de Hulst, 1957). That is, the total Mueller matrix $\mathbf{F}$ for N mechanisms is simply the sum of the N individual Mueller matrices $\mathbf{F}_i$,

$$\mathbf{F} = \sum_{i=1}^{N} \mathbf{F}_i \tag{1}$$

$\mathbf{F}$ can be constructed, therefore, if all $\mathbf{F}_i$ are known. Here only four basic scattering mechanisms are considered.

2.1 Double Bounce Scattering

This mechanism typically models the scattering from the dihedral-corner-reflector-like structures such as the trunk-ground structure in forested areas and the wall-ground structure in urban areas. It has been shown through detailed studies using Stratton-Chu integral techniques, that the scattering matrix $\mathbf{S}$ for the double bounce scattering can be written as (Dong and Richards, 1995a):

$$\mathbf{S}_1 = \begin{bmatrix} S_{hh} & S_{vh} \\ S_{hv} & S_{vv} \end{bmatrix} = \begin{bmatrix} 1 & 0 \\ 0 & \frac{1}{\sqrt{\alpha}} e^{j\delta} \end{bmatrix} S_1 \tag{2}$$

where $S_1 = S_{hh}$ is a function of several parameters such as the incidence angle, dimensions of trunks and walls, and the dielectric properties of trunks, walls and ground surfaces. α and δ are often referred to as the PI (polarisation index, defined as the ratio of HH to VV polarisation responses) and PD (polarisation phase difference, defined as the phase difference between the HH and the VV backscattered fields) values. In the case of perfectly conducting material, $\alpha = 1$ and $\delta = 180^0$ regardless of incidence angle. Usually, α is about $4 \sim 6$ and δ about $140 \sim 160^0$ for the trunk-ground structure, (Dong and Richards, 1995b). The Mueller matrix for the double bounce scattering is (the relationship between the scattering matrix and the symmetrical Mueller matrix is given by Dubois and Norikane (1987), and JPL (1995)),

$$\mathbf{F}_1 = \begin{bmatrix} \frac{\alpha+1}{2\alpha} & \frac{\alpha-1}{2\alpha} & 0 & 0 \\ \frac{\alpha-1}{2\alpha} & \frac{\alpha+1}{2\alpha} & 0 & 0 \\ 0 & 0 & \frac{1}{\sqrt{\alpha}} cos\delta & -\frac{1}{\sqrt{\alpha}} sin\delta \\ 0 & 0 & -\frac{1}{\sqrt{\alpha}} sin\delta & -\frac{1}{\sqrt{\alpha}} cos\delta \end{bmatrix} S_1^2 \tag{3}$$

2.2 Bragg Scattering

Small perturbation techniques have been successfully used to obtain the polarisation dependence from slightly rough surfaces such as sea surfaces (Rice, 1950, Valenzuela, 1967, and Elachi, 1987). The Mueller matrix of the first-order Bragg model is,

$$\mathbf{F}_2 = \begin{bmatrix} \frac{\beta+1}{2\beta} & \frac{\beta-1}{2\beta} & 0 & 0 \\ \frac{\beta-1}{2\beta} & \frac{\beta+1}{2\beta} & 0 & 0 \\ 0 & 0 & \frac{1}{\sqrt{\beta}} & 0 \\ 0 & 0 & 0 & -\frac{1}{\sqrt{\beta}} \end{bmatrix} S_2^2 \tag{4}$$

where β, the mean PI value, is in general less than one. Mathematically,

$$\beta = |\alpha_{hh}/\alpha_{vv}|^2 \tag{5}$$

$$\alpha_{hh} = \frac{\epsilon - 1}{\left(cos\theta + \sqrt{\epsilon - sin^2\theta}\right)^2} \tag{6}$$

$$\alpha_{vv} = (\epsilon - 1)\frac{\epsilon(sin^2\theta + 1) - sin^2\theta}{\left(\epsilon cos\theta + \sqrt{\epsilon - sin^2\theta}\right)^2} \tag{7}$$

θ and ϵ are the incidence angle and the dielectric constant of the surface, respectively. The mean PD value is considered as zero (the Bragg scattering undergoes a single bounce).

2.3 Single Bounce Scattering

This mechanism typically models the direct specular reflections from facets of the ground and/or building roofs perpendicular to the incident direction, and large branches whose axes are perpendicular to the incident direction, and so on. The Mueller matrix for this mechanism is,

$$\mathbf{F}_3 = \begin{bmatrix} 1 & 0 & 0 & 0 \\ 0 & 1 & 0 & 0 \\ 0 & 0 & 1 & 0 \\ 0 & 0 & 0 & -1 \end{bmatrix} S_3^2 \tag{8}$$

The co-polarised response from forest crown volume backscattering can be included in this mechanism. If the orientations of leaves, twigs and small branches are assumed to be uniformly distributed, the backscattering response will be independent of polarisation, giving the same HH and VV response. The backscattering from the trihedral-corner-reflector-like, wall-wall-ground structure can also be classified into this mechanism, since the scattering undergoes odd bounces.

2.4 Cross Scattering

The polarimetric response of a point or distributed target in general can be decomposed into co- and cross-polarised responses. If we are only interested in the total cross-polarised component, we can assume theoretically that the total cross-polarised response is caused by a hypothetical cross scattering mechanism whose scattering matrix is,

$$\mathbf{S}_4 = \begin{bmatrix} 0 & 1 \\ 1 & 0 \end{bmatrix} S_4 \tag{9}$$

and the corresponding Mueller matrix of the cross scattering mechanism can be written as,

$$\mathbf{F}_3 = \begin{bmatrix} 1 & 0 & 0 & 0 \\ 0 & -1 & 0 & 0 \\ 0 & 0 & 1 & 0 \\ 0 & 0 & 0 & 1 \end{bmatrix} S_4^2 \tag{10}$$

3 ALGORITHM

The total Mueller matrix is the sum of the Mueller matrices for the above individual mechanisms. This gives,

$$f_{11} = \frac{\alpha+1}{2\alpha}S_1^2 + \frac{\beta+1}{2\beta}S_2^2 + S_3^2 + S_4^2 \tag{11}$$

$$f_{12} = \frac{\alpha-1}{2\alpha}S_1^2 + \frac{\beta-1}{2\beta}S_2^2 \tag{12}$$

$$f_{22} = \frac{\alpha+1}{2\alpha}S_1^2 + \frac{\beta+1}{2\beta}S_2^2 + S_3^2 - S_4^2 \tag{13}$$

$$f_{33} = \frac{cos\delta}{\sqrt{\alpha}}S_1^2 + \frac{1}{\sqrt{\beta}}S_2^2 + S_3^2 + S_4^2 \tag{14}$$

$$f_{34} = -\frac{sin\delta}{\sqrt{\alpha}}S_1^2 \tag{15}$$

$$f_{44} = -\frac{cos\delta}{\sqrt{\alpha}}S_1^2 - \frac{1}{\sqrt{\beta}}S_2^2 - S_3^2 + S_4^2 \tag{16}$$

$$S_i^2 \geq 0 \qquad i = 1, \cdots, 4 \tag{17}$$

The left sides of (11)-(16) are the elements of the Mueller matrix measured by the polarimetric radar system. S_i^2 $(i = 1, \cdots, 4)$ are the four unknowns to be decided. The optimal solution of (11)-(17) can be found using the WLS method. After the unknowns are obtained, the simulated Muller matrix

$$\mathbf{F} = \mathbf{F}_1 + \mathbf{F}_2 + \mathbf{F}_3 + \mathbf{F}_4 \tag{18}$$

can be reconstructed, and the co- and cross-polarisation responses predicted by the model are,

$$\sigma_{hh}^0 = 4\pi(S_1^2 + S_2^2 + S_3^2) \tag{19}$$

$$\sigma_{vv}^0 = 4\pi(S_1^2/\alpha + S_2^2/\beta + S_3^2) \tag{20}$$

$$\sigma_{vh}^0 = \sigma_{hv}^0 = 4\pi S_4^2 \tag{21}$$

4 RESULTS AND DISCUSSIONS

In August-September 1993, the NASA/JPL AirSAR quad-polarised system flew approximately 60 test sites in Australia. Two of them are used to test the model. One is the Gippsland site covered by native eucalypts, farmland and pine plantations while the other, the Sydney site, has typical urban features, such as commercial and residential buildings or a mixture. An ocean water area is also covered by the second site. The incidence angle varies from about 30^0 in near range to 60^0 in far range. Since the mean value eliminates the speckle effects, and characterises the features of the distributed targets, sub-blocks, normally more than 2000 pixels, are used for the simulation. The size of a pixel is about $6 \times 6\ m^2$.

To obtain the optimal decomposition, the values of α, β and δ have to be given. For forests in the first site, we assume that the double bounce scattering is caused by the trunk-ground structure. Therefore, $\alpha = 4$ and $\delta = 150^0$ are chosen. For the urban areas in the second site, we assume that the double bounce scattering is caused by both metallic and dielectric materials, thus $\alpha = 2.5$ and $\delta = 165^0$ are chosen. The choice of β is a little more complicated, because it varies very much with the incidence angle. In the simulation, β varies in the region of $0.5 \sim 0.1$ according to the incidence angle and the dielectric constants.

In our simulation, all the weighting factors in the method of WLS are chosen to be the same for simplicity, resulting in the decomposed value being identical to the measured value for HV (VH) polarisation. In the following examples, therefore, the decomposed cross scattering components will not be mentioned further.

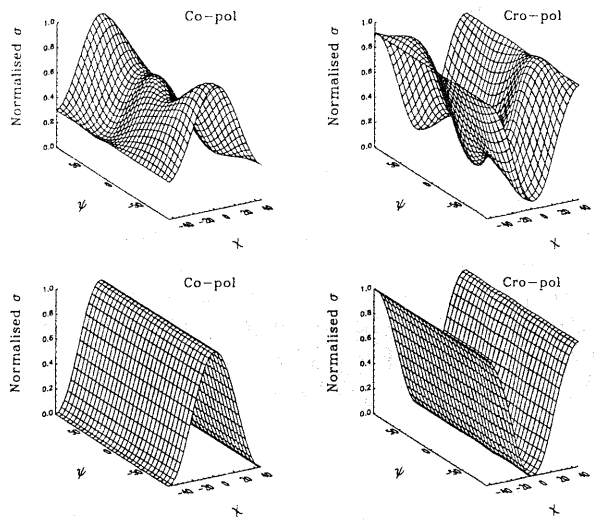

Figure 1: Top: Measured P-band polarisation signatures from buildings facing radar at incidence angle of 30^0. Bottom: theoretical polarisation signatures by single bounce scattering.

4.1 Residential Buildings

The backscattering from residential buildings in urban areas could be dominated by a single bounce from building roofs and/or a double bounce from the wall-ground structures depending on buildings' orientation and radar's incidence angle. Two groups of residential buildings in the Sydney region are selected for comparison. These two groups of buildings are all facing radar and similar to one another, except that the radar's in-

cidence angles are different because one group is in the near range and the other in the far range. It is found that for buildings in the near range where the incidence angle is about 30^0, the backscattering is dominated by single bounce scattering. According to our observation, the roofs of most of buildings, consisting of plain tiles, are tilted about $30 \sim 35^0$ from vertical. Therefore, strong specular reflections from the roofs are expected. Figure 1 shows the measured P-band polarisation signatures by these buildings at the incidence angle of 30^0. Shown in the figure are also theoretical polarisation signatures by single bounce scattering for comparison. In contrast, when the incidence angle becomes 60^0 for the buildings in the far range, the roofs are not perpendicular to the radar any more. What the radar measures in this case is a strong double bounce scattering from the wall-ground structures. Figure 2 shows the observed P-band polarisation signature by these buildings at the incidence angle of 60^0. Shown in the figure are also theoretical polarisation signatures by double bounce scattering from a wall-ground structure for comparison.

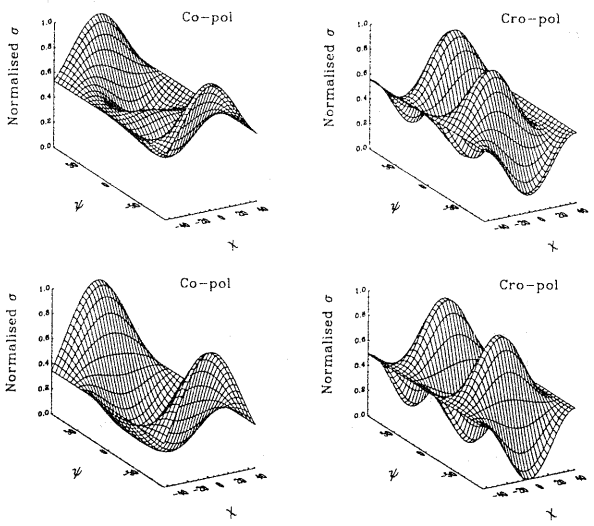

Figure 2: Top: Measured P-band polarisation signatures from buildings facing radar at incidence angle of 60^0. Bottom: theoretical polarisation signatures by double bounce scattering.

Tables 1 and 2 list the percentages of single, double and Bragg scattering components of the HH polarisation for these two groups of residential buildings at P-, L- and C-bands. The error between the predicted and the measured values is also given in the tables. It can been seen that while a dominant single bounce scattering component is decomposed for the buildings at the incidence angle of 30^0, a strong double bounce scattering component is attributed to the buildings at the incidence angle of 60^0.

One can see from Table 1 or Table 2 that the decom-

Table 1: Scattering components as a percentage of the total HH backscattering response for residential buildings at incidence angle of 30^0.

Band	Single%	Double %	Bragg %	Error %
P	65	35	0	3.4
L	63	37	0	5.1
C	59	41	0	2.8

Table 2: Scattering components as a percentage of the total HH backscattering response for residential buildings at incidence angle of 60^0.

Band	Single %	Double %	Bragg %	Error %
P	25	75	0	3.2
L	22	78	0	-5.4
C	30	70	0	6.8

positions are similar at all three bands, which implies that the polarisation signatures at all three bands are similar for each group of buildings. One of the possible reasons to explain this is that the large rigid structures of built targets may appear not significantly different to P-, L- and C-band radars. Therefore, statistically, all three band radars capture similar polarisation signatures. As will be seen in the following subsections, the situation for forested areas is totally different.

4.2 Forests

The decomposition for native eucalypts is listed in Table 3. The components of double bounce scattering decrease from P- to C-band, because foliage attenuation increases with an increase of the frequency. It is the foliage attenuation that masks the double bounce scattering from the trunk-ground structures. On the other hand, the single bounce components increase from P- to C-band, as the backscattering from the top layer increases with increase in frequency. Figure 3 shows the co- and cross-polarisation signatures for the native eucalypts at P-, L- and C-bands. It can be observed that while the double bounce scattering dominates the P- and L-band signatures, the single bounce scattering features in the C-band signature. In addition, pedestals (co-polarisation at $\chi = \pm 45^0$) are high for all bands. Physically, this means that the responses of RR (right-handed transmission, right-handed receiving) and LL (left-handed transmission and left-handed receiving) circular polarisations are significant. A field of right-handed circular rotation becomes a field of left-handed circular rotation after a single bounce of the specular reflection and vice versa for pure conducting material. The VH (HV) compo-

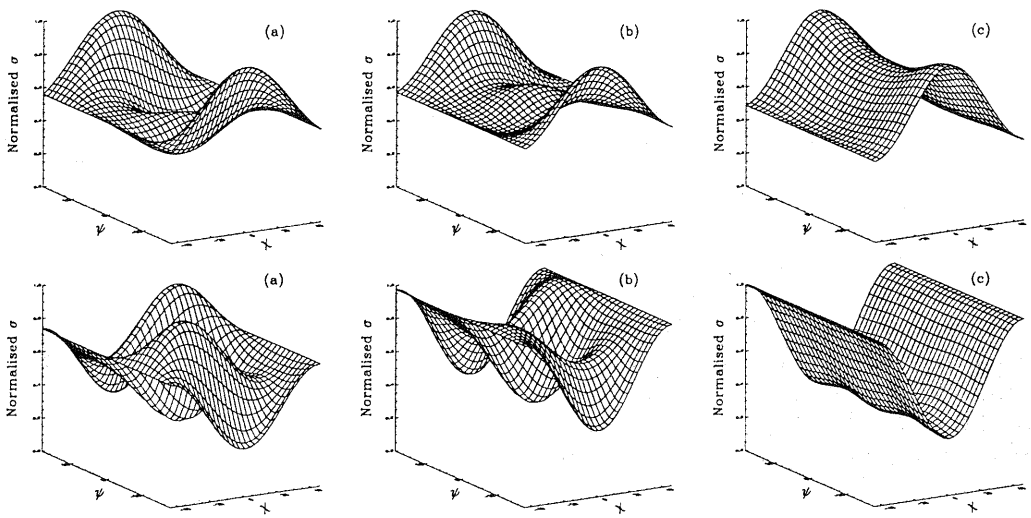

Figure 3: Co- (top) and cross-polarisation (bottom) signatures for native eucalypts at (a) P-, (b) L- and (c) C-bands measured by NASA/JPL AirSAR system.

nent is also responsible for the pedestals. In general, therefore, the higher the pedestal is, the more the double bounce scattering and the cross-polarised components. The result that a significant part of the double bounce scattering is decomposed at C-band, seems in conflict with the common understanding that C-band mainly interacts with the crown layer. There is a possible reasons for this result. Eucalypts in the site are sparse, and their crown closure is less than 25%. It is possible, therefore, that the double bounce scattering between the underlying vegetation and the ground surface is also captured. However, for whatever reason, according to the theory, a significant double bounce scattering component will be decomposed if there is a significant pedestal in the signature.

Table 3: Scattering components as a percentage of the total HH backscattering response for native eucalypts at incidence angle of 45^0.

Band	Single %	Double %	Bragg %	Error %
P	17	77	6	0.1
L	24	67	10	1.4
C	47	44	9	0.6

4.3 Ocean

Table 4 gives the percentages of the single, double and Bragg scattering components decomposed from HH polarisations for the ocean water at P- L- and C-bands.

In this example, P-band predicts a strong Bragg scattering component, but less in the other two bands.

Table 4: Scattering components as a percentage of the total HH backscattering response for ocean water at the incidence angle of 35^0.

Band	Single %	Double %	Bragg %	Error %
P	0	38	62	-5.8
L	49	43	7	0.0
C	31	55	14	0.0

It is understood that the Bragg scattering is frequency dependent, and relates to the frequency of both gravity and breaking waves on the ocean surface. As shown in Figure 4, only P-band captured a strong Bragg scattering component in this example.

4.4 Reconstruction of Polarisation Signatures

So far the decomposition of the HH response for various types of targets has been shown. The error between the measured values and the predicted values is usually less than 5% in most cases. In fact the backscattering response of an arbitrary polarisation ellipse can also be retrieved from polarimetric SAR data in addition to the linear polarisation of HH, VV and VH. To demonstrate the precision of the proposed decomposition technique for any polarisation, polarisation signatures using the measured Mueller matrix and the reconstructed Mueller matrix given by (18) are compared. It is found that the error between the measured polarisation signature and the simulated polarisation signature is less than 15% for most cases, at all bands. Figures 5–7 show both the co- and cross-

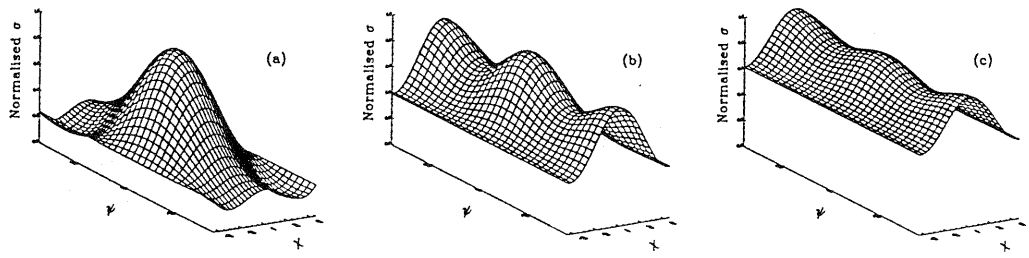

Figure 4: Co-polarisation signatures of ocean water at (a) P-, (b) L- and (c) C-bands measured by NASA/JPL AirSAR system.

polarisation signatures plotted using the measured and simulated Mueller matrices for farmland, residential areas and the ocean water at P-band. The absolute differences between the measured and simulated signatures are also shown in the figures.

5 CONCLUSIONS

A method of optimal decomposition for radar polarisation signatures has been developed. In the model the backscattering consists of single, double, Bragg and cross backscattering components and the Mueller matrix is the sum of the Mueller matrices of these four scattering mechanisms. The technique of the Weighted Least Squares is then used to find the optimal combination of these four components. The method has been tested using NASA/JPL AirSAR data. The results of decomposition generally agree with the accepted understanding of radar backscatter, and in most cases, the accuracy of the decomposition is more than 95% for linear polarisations and more than 85% for any other polarisations. It should be noted that the decomposition is not unique and is dependent on the basic model assumptions. However, the optimal decomposition method itself seems robust. It is expected that if better model assumptions are proposed, a better decomposition can be obtained. The distinct polarisation signatures of the land surface tested and the ability to understand and predict them from a limited number of scattering mechanisms suggested that these signatures can be used as a basis for land use classification.

6 REFERENCES

Cloude, S. R., 1991. Optimisation methods in radar polarimetry. Proceedings of ICAP '91 Conference, pp. 392–395. London: The Institution.

Dong, Y., and Richards, J. A., 1995a. Studies of the cylinder–ground double bounce scattering mechanism in forest backscatter models. IEEE Trans on Geoscience and Remote Sensing, 33(1), pp. 229-231.

Dong, Y., and Richards, J. A., 1995b. Forest discrimination using SAR multifrequency and multipolarisation data. Proceedings of IGARSS '95 Symposium. Noordwijk: ESA Scientific & Tech.

Dubois, P. C., and Norikane, L., 1987. Data volume reduction for imaging radar polarimetry. Proceedings of IGARSS '87 Symposium, pp. 691–696. Noordwijk: ESA Scientific & Tech.

Durden, S. L., Klein, J., and Zebker, H. A., 1991. Polarimetric radar measurements of a forested area near Mt. Shasta. IEEE Trans on Geoscience and Remote Sensing, 29(3), pp. 444-450.

Elachi, C., 1987. Introduction to the Physics and Techniques of Remote Sensing. New York: John Wiley and Sons Inc..

Evans, D. A., Farr, T. G., van Zyl, J. J., and Zebker, H. A., 1988. Radar polarimetry: Analysis tools and application. IEEE Trans on Geoscience and Remote Sensing, 26(6), pp. 774-798.

Freeman, A., and Durden, S., 1992. A three–component scattering model to describe polarimetric SAR data. Proceedings of Radar Polarimetry: 23-24 July 1992, San Diego, California, pp. 213–224. Washington: SPIE.

JPL, 1995. AirSAR integrated processor documentation: Data formats, version 0.01. California: Jet Propulsion Laboratory.

Kwok, R., Rignot, E. J. M., Way, J., Freeman, A., and Holt, J., 1994. polarisation signatures of frozen and thawed forests of varying environmental state. IEEE Trans on Geoscience and Remote Sensing, 32(2), pp. 371–381.

Pierce, L. E., Ulaby, F. T., Sarabandi, K., and Dobson, M. C., 1994. Knowledge-based classification of polarimetric SAR images. IEEE Trans on Geoscience and Remote Sensing, 32(5), pp. 1081-1086.

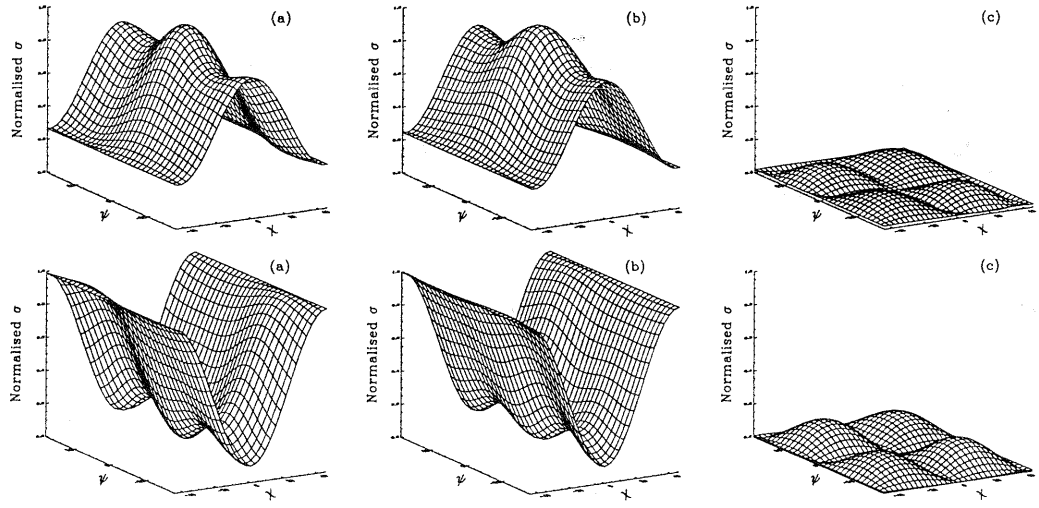

Figure 5: polarisation signature (top: co-polarisation and bottom: cross-polarisation) comparison using the measured and simulated Mueller matrices for unploughed farmland covered with short grass in Gippsland at P-band: (a) measured, (b) simulated and (c) absolute difference.

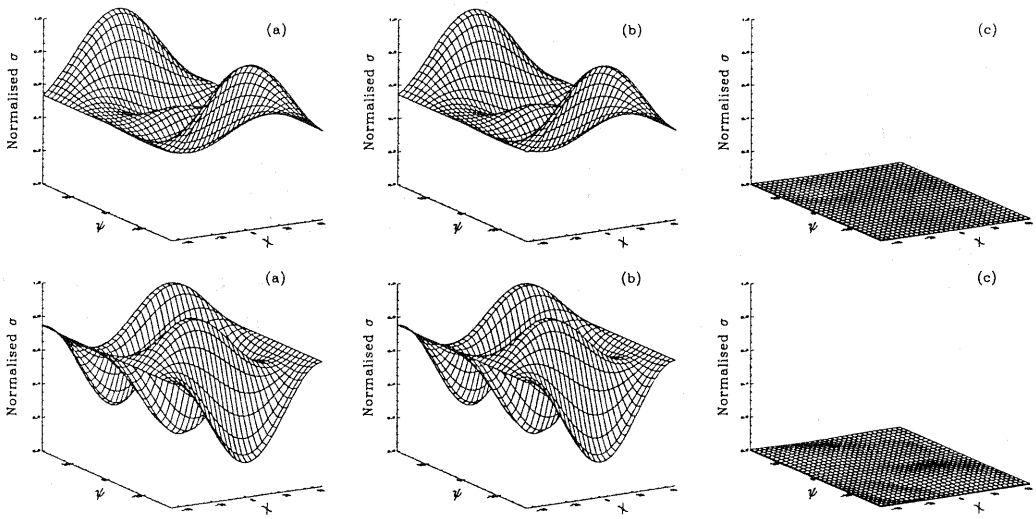

Figure 6: polarisation signature (top: co-polarisation and bottom: cross-polarisation) comparison using the measured and simulated Mueller matrices for residential areas in Sydney at P-band: (a) measured, (b) simulated and (c) absolute difference.

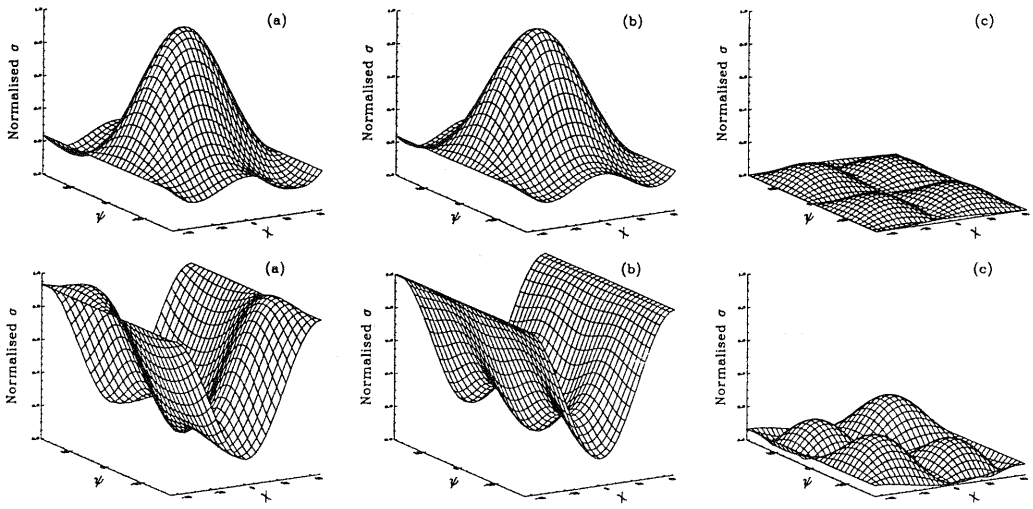

Figure 7: polarisation signature (top: co-polarisation and bottom: cross-polarisation) comparison using the measured and simulated Mueller matrices for the ocean water in Sydney at P-band: (a) measured, (b) simulated and (c) absolute difference.

Rice, S. O., 1951. Reflection of electromagnetic waves from slightly rough surface. In Kline, M., The Theory of Electromagnetic Waves. New York: John and Wiley Inc..

Ulaby, F. T., and Elachi C. (editors) 1990. Radar Polarimetry for Geoscience Applications. Boston: Artech House, Inc..

Valenzuela, G. R., 1967. Depolarisation of EM waves by slightly rough surfaces. IEEE Trans on Antennas and Propagation, AP-15(4), pp. 552-557.

van de Hulst, H. C., 1957. Light Scattering by Small Particles. New York: John Wiley and Sons Inc..

van Zyl, J. J., 1989. Unsupervised classification of scattering behaviour using radar polarimetry data. IEEE Trans on Geoscience and Remote Sensing, 27(1), pp. 36–45.

Zebker, H. A., and van Zyl, J. J., 1991. Imaging radar polarimetry: a review. Proceedings of IEEE, 99(11), pp. 1583–1605.